SCIENTIFIC REPORTS

OPEN

Relationship between ion migration and interfacial degradation of CH$_3$NH$_3$PbI$_3$ perovskite solar cells under thermal conditions

Seongtak Kim[1], Soohyun Bae[1], Sang-Won Lee[1], Kyungjin Cho[1], Kyung Dong Lee[1], Hyunho Kim[1], Sungeun Park[1], Guhan Kwon[2], Seh-Won Ahn[2], Heon-Min Lee[2], Yoonmook Kang[3], Hae-Seok Lee[3] & Donghwan Kim[1]

Organic-inorganic hybrid perovskite solar cells (PSCs) have been extensively studied because of their outstanding performance: a power conversion efficiency exceeding 22% has been achieved. The most commonly used PSCs consist of CH$_3$NH$_3$PbI$_3$ (MAPbI$_3$) with a hole-selective contact, such as 2,2′,7,7′-tetrakis(*N*,*N*-di-*p*-methoxyphenylamine)-9,9-spiro-bifluorene (spiro-OMeTAD), for collecting holes. From the perspective of long-term operation of solar cells, the cell performance and constituent layers (MAPbI$_3$, spiro-OMeTAD, etc.) may be influenced by external conditions like temperature, light, etc. Herein, we report the effects of temperature on spiro-OMeTAD and the interface between MAPbI$_3$ and spiro-OMeTAD in a solar cell. It was confirmed that, at high temperatures (85 °C), I$^-$ and CH$_3$NH$_3^+$ (MA$^+$) diffused into the spiro-OMeTAD layer in the form of CH$_3$NH$_3$I (MAI). The diffused I$^-$ ions prevented oxidation of spiro-OMeTAD, thereby degrading the electrical properties of spiro-OMeTAD. Since ion diffusion can occur during outdoor operation, the structural design of PSCs must be considered to achieve long-term stability.

Since the advent of organic-inorganic hybrid perovskite solar cells (PSCs) in 2009, such cells have been extensively researched. PSCs offer the benefits of a simple and cost-effective fabrication process and outstanding power conversion efficiency[1–5]. Recently, PSCs with >22% efficiency were reported; however, the long-term stability of these types of solar cells impedes their commercialization[6]. High-efficiency PSCs consist of a perovskite absorber, such as MAPbI$_3$ or Cs$_x$(MA$_y$FA$_{1-y}$)$_{(1-x)}$Pb(I$_z$Br$_{1-z}$)$_3$, with respective electron- and hole-selective contacts such as mesoporous TiO$_2$ (m-TiO$_2$) and 2,2′,7,7′-tetrakis(*N*,*N*-di-*p*-methoxyphenylamine)-9,9-spiro-bifluorene (spiro-OMeTAD)[5, 7].

An efficiency drop has frequently been reported for these PSCs. The primary causes of degradation of the performance of solar cells are widely known to be related to external conditions, such as moisture[8, 9], temperature[10, 11], UV light[12, 13], etc. In addition, issues related to internal factors, such as ion migration[14, 15], interfacial reactions[16], etc., are stated as causes of insufficient long-term stability of PSCs. Solar cells must exhibit stability to the external conditions stated above to operate efficiently for several decades. Since the temperature of the solar cell can reach up to 85 °C during typical operating conditions, thermal stability is important for long-term operation in particular.

In the m-TiO$_2$/MAPbI$_3$/spiro-OMeTAD structure, spiro-OMeTAD acts as a hole collector and also protects MAPbI$_3$ from the external environment. In recent research, the chemical structure of spiro-OMeTAD was modified to increase its glass transition temperature and conductivity to enhance its thermal stability and hole collection ability[17]. To protect the perovskite from moisture, various hole transporting materials (HTMs), such as hydrophobic and inorganic materials, have been developed resulting in increased long-term stability[18–21]. They

[1]Department of Materials Science and Engineering, Korea University, 145 Anam-ro, Seongbuk-gu, Seoul, 02841, Republic of Korea. [2]Materials & Production engineering Research Institute, LG Electronics, 38 Baumoe-ro, Seocho-gu, Seoul, 06763, Republic of Korea. [3]KU·KIST Green School Graduate School of Energy and Environment, Korea University, 145 Anam-ro, Seongbuk-gu, Seoul, 02841, Republic of Korea. Correspondence and requests for materials should be addressed to Y.K. (email: ddang@korea.ac.kr) or H.-S.L. (email: lhseok@korea.ac.kr) or D.K. (email: solar@korea.ac.kr)
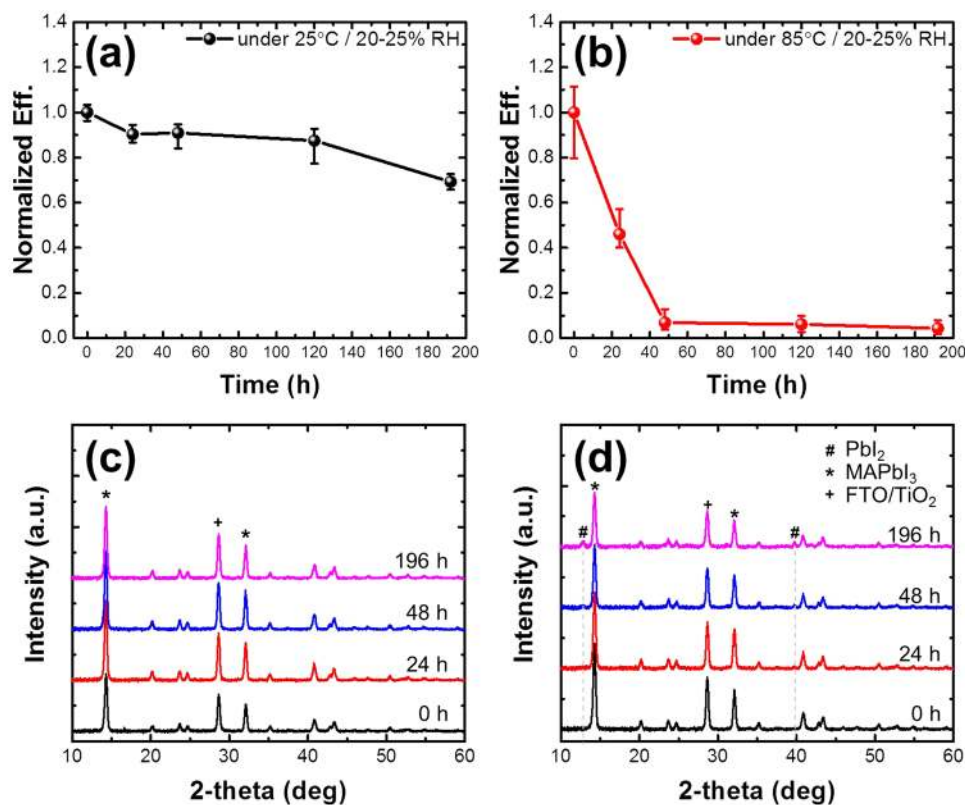
Figure 1. Long-term stability of MAPbI$_3$ PSCs and perovskite films: power conversion efficiency at (**a**) 25 °C and (**b**) 85 °C with time and X-ray diffraction pattern of FTO/TiO$_2$/MAPbI$_3$/spiro-OMeTAD structure at (**c**) 25 °C and (**d**) 85 °C with time.

enhanced not only the long-term stability of PSCs, but also the electrical contact of perovskite/HTM interfaces. Since spiro-OMeTAD suffers from low electrical conductivity due to the large intermolecular distances[22, 23], dopants like Li-bis(trifluoromethanesulfonyl) imide (Li-TFSI) and tert-butylpyridine (TBP) have been added to spiro-OMeTAD to induce the doping effect[24]. It has been reported that perovskite materials may be decomposed by the liquids used for deposition of HTMs, such as TBP and acetonitrile[25, 26]; thus, HTM-free PSCs have been fabricated to enhance their long-term stability[27]. However, these kinds of PSCs have lower efficiencies than PSCs with traditional structures including of HTM.

The relationship between MAPbI$_3$ and spiro-OMeTAD was evaluated; the results showed that under photo-irradiation with >450-nm wavelength light, MAPbI$_3$ assisted the oxidation of spiro-OMeTAD[28]. In contrast, introduction of CH$_3$NH$_3$I (MAI) into spiro-OMeTAD can reduce the oxidized spiro-OMeTAD (spiro-OMeTAD$^+$)[29]. Thus, studies on the interfacial reaction between MAPbI$_3$ and spiro-OMeTAD under various external environments are needed to achieve long-term stability.

In this study, the degradation of spiro-OMeTAD and the MAPbI$_3$/spiro-OMeTAD interface due to ion migration is investigated with variation of the thermal conditions. While there was no significant change of MAPbI$_3$ at 85 °C within a short time, spiro-OMeTAD and the interface between MAPbI$_3$/spiro-OMeTAD were affected because of migration of I$^-$ and MA$^+$. Analysis of the results revealed that PSCs can be thermally degraded due to ion migration, thereby reducing the conductivity and hole collection ability of spiro-OMeTAD.

Results and Discussions

A methylammonium lead iodide perovskite layer was obtained by spin-coating using a one-step solution process via dripping diethyl ether[7]. In this study, the thermal behavior was evaluated based on reverse scanning of the solar cells with ~16% power conversion efficiency (Figure S1). The external quantum efficiency (EQE) was nearly 80% at wavelengths of 400–600 nm. No PbI$_2$ peak (12.6° (001)) was observed in the XRD pattern of the prepared m-TiO$_2$/MAPbI$_3$ substrate, while typical peaks for MAPbI$_3$ were observed at 14.1° (110), 19.9° (112), 23.5° (211), and 24.5° (202).

Several researchers have evaluated the thermal stability of MAPbI$_3$ PSCs with various structures[30, 31]. However, except for the HTM-free structure, most PSCs employing an organic HTM (such as spiro-OMeTAD) degraded under thermal stress. The thermal stabilities of the PSCs developed herein were evaluated at 25 and 85 °C under ambient conditions as a function of time (Fig. 1a,b). At 25 °C, the conversion efficiency dropped by about 30% after 196 h; in contrast, at 85 °C, the conversion efficiency declined by almost 100% after 48 h. For comparison of the analysis of the phase changes that affect the solar cell efficiency, XRD patterns were acquired at 25 and 85 °C as a function of time, as shown in Fig. 1c,d. At 25 °C, the XRD pattern remained almost unchanged over time. At
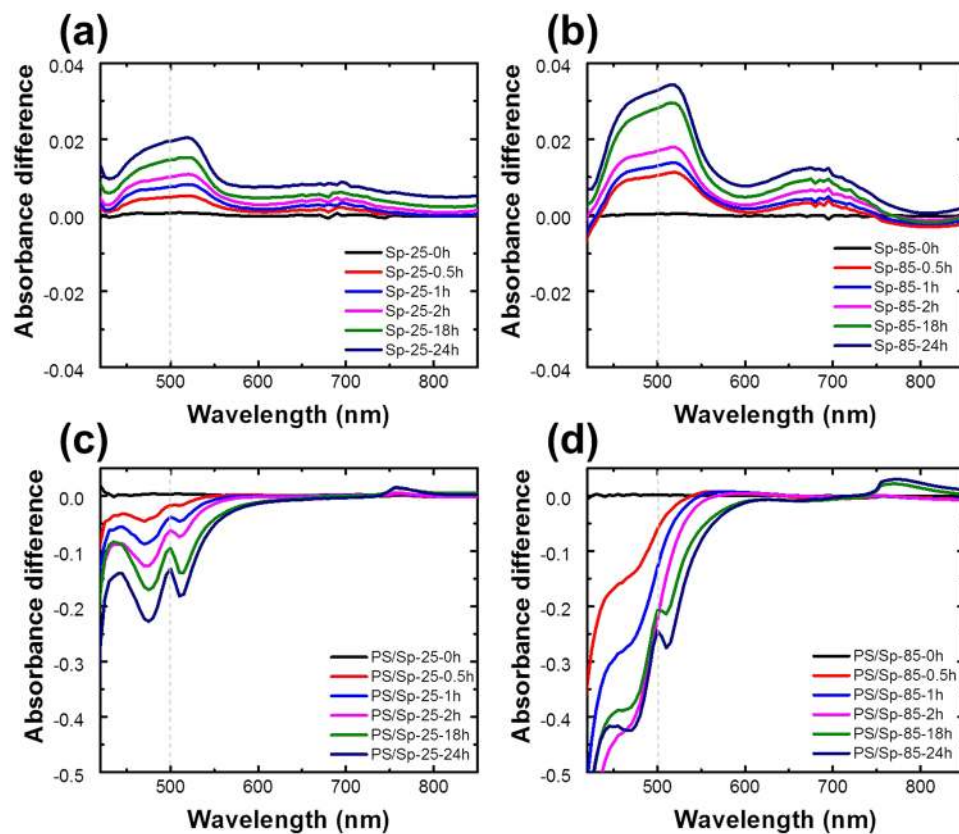
Figure 2. Changes in the absorbance of spiro-OMeTAD at (**a**) 25 °C and (**b**) 85 °C with time. Changes in the absorbance of MAPbI$_3$/spiro-OMeTAD at (**c**) 25 °C and (**d**) 85 °C with time.

85 °C, the XRD patterns remained unaffected until 48 h, at which point decomposition of the MAPbI$_3$ film was observed based on the appearance of a PbI$_2$ peak. In a previous study, the long-term and high-temperature stability were found to be influenced by humidity, a pinhole in the spiro-OMeTAD film, and the hygroscopic nature of Li-TFSI[11, 32]. The reports showed that exposure of the cells to high relative humidity under thermal conditions for a long period of time resulted in decomposition of the perovskite, not only because of penetration of water molecules, but also because of thermal degradation of the MAPbI$_3$ perovskite film. In another study on MAPbI$_3$ solar cells with remnant PbI$_2$, moderate efficiencies (5–10%) were achieved relative to that of MAPbI$_3$, even though PbI$_2$ was fairly evenly distributed in those films based on the XRD data[33, 34]. One reported advantage of the remnant PbI$_2$ was that it can act as a passivation layer for the MAPbI$_3$ grains, resulting in higher solar cell efficiency rather than a drop in the efficiency[34]. However, from the XRD data used to compare the fast efficiency drop at 85 °C over time, we propose that the degradation of the solar cell performance was not only influenced by decomposition of the perovskite due to the thermal conditions, but also other factors such as degradation of the HTMs.

To elucidate the high-temperature (85 °C) behavior of spiro-OMeTAD, the variations of the absorbance of the spiro-OMeTAD film at 25 and 85 °C as a function of time were evaluated, as shown in Fig. 2a,b. Spiro-OMeTAD can be oxidized to spiro-OMeTAD$^+$ by additives like Li-TFSI and external factors such as oxygen and light[24, 28]. Formation of spiro-OMeTAD$^+$ from spiro-OMeTAD is indicated by an absorption peak in a particular wavelength region. In a previous report, when spiro-OMeTAD was oxidized to spiro-OMeTAD$^+$, the optical absorption at around 500 nm increased and was accompanied by the development of electrical conductivity[24, 35]. Figure 2a shows that, at 25 °C, the absorbance around 500 nm increased as a function of time in the spiro-OMeTAD film only. Since the measurement was performed under dark and ambient conditions, the oxidation was due to oxygen and Li-TFSI. When the sample was treated at 85 °C, the oxidation reaction accelerated (Fig. 2b). The increase in the absorbance peak of spiro-OMeTAD$^+$ over time indicates that spiro-OMeTAD was oxidized at both temperatures, but to a greater extent at 85 °C.

As mentioned above, spiro-OMeTAD containing MAPbI$_3$ was observed to undergo enhanced oxidation under irradiation with >450-nm wavelength light[28]. This indicates that not only external conditions, but also MAPbI$_3$, can affect the properties of spiro-OMeTAD. In conventional PSCs, since spiro-OMeTAD is tightly affixed to MAPbI$_3$ as an HTM, spiro-OMeTAD can be influenced by MAPbI$_3$ at high temperatures. The effects of temperature and time on the absorbance of MAPbI$_3$/spiro-OMeTAD are summarized in Fig. 2c,d. At 25 °C, the specific absorbance peak appeared at ~500 nm after 30 min. The presence of this peak indicates that spiro-OMeTAD was oxidized at 25 °C under ambient conditions, regardless of the presence of MAPbI$_3$. In contrast, at 85 °C, the absorption peak at ~500 nm did not appear until 2 h of treatment, and this specific peak was observed after 18 h when MAPbI$_3$/spiro-OMeTAD was treated at 85 °C. Thus, it can be deduced that MAPbI$_3$ influences the
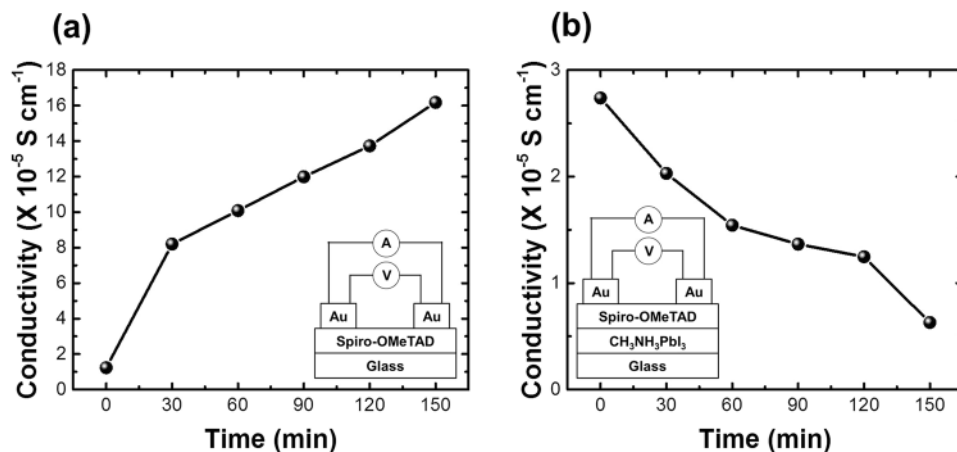
Figure 3. Dark conductivity of (**a**) spiro-OMeTAD and (**b**) MAPbI$_3$/spiro-OMeTAD at 85 °C with time. Four-point probe measurement was used for the conductivity analysis. Inset shows structures for the measurement of conductivity of spiro-OMeTAD, glass/spiro-OMeTAD/Au, and glass/MAPbI$_3$/spiro-OMeTAD/Au.

oxidation of spiro-OMeTAD at high temperatures. Since oxidation and reduction can affect the conductivity of spiro-OMeTAD, the dependence of the conductivity of spiro-OMeTAD on MAPbI$_3$ at 85 °C was evaluated via a four-point probe measurement.

As shown in the inset in Fig. 3a,b, glass/spiro-OMeTAD/Au and glass/MAPbI$_3$/spiro-OMeTAD/Au structures were used for the measurements. The initial difference in values was due to the different surface morphologies of glass and MAPbI$_3$ despite the same spin coating condition. Since the thickness of spiro-OMeTAD was about 200–250 nm in this study, the conductivity of $1-3 \times 10^{-5}$ Scm^{-1} for spiro-OMeTAD was similar to previous results[28, 36]. Figure 3a,b show the variation of the conductivity of spiro-OMeTAD with time at 85 °C for each structure. In the spiro-OMeTAD film, the conductivity of spiro-OMeTAD increased upon treatment at 85 °C, whereas the conductivity of spiro-OMeTAD in the MAPbI$_3$/spiro-OMeTAD structure decreased. Comparison of this absorption data with that of spiro-OMeTAD (Fig. 2b) revealed that the conductivity of spiro-OMeTAD without MAPbI$_3$ increased because of oxidation of spiro-OMeTAD at 85 °C. On the other hand, the decreased conductivity of MAPbI$_3$/spiro-OMeTAD indicates that oxidation of spiro-OMeTAD was hindered because of an interfacial reaction between MAPbI$_3$ and spiro-OMeTAD at 85 °C (Fig. 3b). As mentioned above, a decrease of the conductivity of spiro-OMeTAD due to incorporation of MAI was reported[29]. A previous study reported that, since iodine ions, such as those derived from MAI, are highly coordinating, the decreased polaronic band resulted in reduction of spiro-OMeTAD$^+$. Iodide ions can move easily because of their very low ion migration energy (0.16–0.43 eV)[15, 37, 38]. At high temperatures, the mobile iodide ions easily diffuse to MAPbI$_3$ as well as nearby layers, such as the spiro-OMeTAD layer, thereby changing the electrical properties of spiro-OMeTAD. Similar conductivity behaviors of spiro-OMeTAD were also observed with increasing temperature in the same structure (Figure S2). With increasing temperature, the conductivity of spiro-OMeTAD without MAPbI$_3$ increased, whereas that in the MAPbI$_3$/spiro-OMeTAD structure did not. Since the extent of ion migration is proportional to temperature, the decreased conductivity reflects the possibility of the migration of ions such as I$^-$ and MAI with increasing temperature. Based on these results, we proposed that thermally diffused I$^-$ and MAI negatively influence spiro-OMeTAD at high temperatures.

When spiro-OMeTAD is not sufficiently oxidized, PSCs exhibit very low conversion efficiencies[39]. Oxidation of spiro-OMeTAD not only increased the conductivity, but also increased the charge collection because of a shift of the energy level. Thus, to promote oxidation of spiro-OMeTAD, Li-TFSI was added to spiro-OMeTAD. The EQEs of the thermally degraded PSCs were compared with that of the pristine PSCs without Li-TFSI (Figure S3). In the case of the PSCs without Li-TFSI, because spiro-OMeTAD was not sufficiently oxidized, a low EQE response between 500–800 nm was obtained. The EQE curve of the degraded PSCs was similar to that of the PSCs without Li-TFSI (i.e., not sufficiently oxidized). Thus, this result indicates that, although MAPbI$_3$ was not excessively decomposed, the efficiency of the PSCs may be reduced because of reduction of spiro-OMeTAD, leading to decreased hole collection.

Recently, transmission electron microscopy (TEM) and energy-dispersive X-ray spectroscopy (EDX) were used to monitor the effects of increasing the temperature up to 300 °C (using *in-situ* TEM) on spiro-OMeTAD[40]. Iodide ions began diffusing into spiro-OMeTAD at 175 °C because of the high mobility of the iodide ions. These mobile iodide ions originate from MAPbI$_3$ or excess MAI present during formation of the perovskite film. In this study, the iodide ions were also observed via TEM analysis of the MAPbI$_3$/spiro-OMeTAD interface (Fig. 4). EDX line mapping of the interface is displayed in the inset. In contrast with the TEM and EDX data, it is evident that iodine was present in spiro-OMeTAD: iodine was present in the fresh sample of spiro-OMeTAD to a depth of <20 nm at the MAPbI$_3$/spiro-OMeTAD interface (Fig. 4a). This iodine may be derived from several sources such as dissolution of the MAPbI$_3$ surface during spin-coating of spiro-OMeTAD or disconnection between MAI and PbI$_2$ during annealing of the MAPbI$_3$ film. Interestingly, migration of iodine to a depth of ~80 nm into
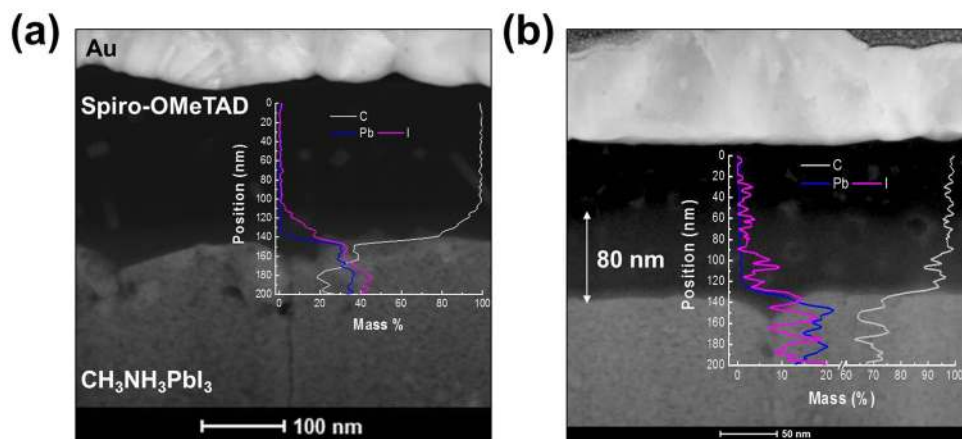
Figure 4. High-angle annular dark-field (HAADF) scanning transmission electron microscopy (TEM) images showing cross-sectional views of the MAPbI$_3$/spiro-OMeTAD interface: (**a**) pristine and (**b**) thermally stressed at 85 °C for 2 h. Inset shows EDX line maps for lead and iodine. Contrast images and EDX display the presence of iodine.

spiro-OMeTAD was observed only with treatment at 85 °C for 2 h (Fig. 4b). This iodine migration at 85 °C was elucidated and confirmed by time-of-flight secondary ion mass spectrometry (TOF-SIMS, Figure S4).

The origin of the migratory iodide ions remained unconfirmed. Iodine moved along the grain boundary (GB) of the MAPbI$_3$ grains under an electric field[41]. The iodine and lead profiles of a MAPbI$_3$ GB sample degraded at 85 °C are shown in Figure S5. While the atomic ratio of lead was constant, that of iodine in the GB declined. Furthermore, the atomic ratio of iodine decreased to a greater extent while moving toward spiro-OMeTAD. Since iodide ions migrate faster in the GB than in bulk MAPbI$_3$[41], the iodide ions in the MAPbI$_3$ films can also migrate at high temperatures. Therefore, we propose that the migratory iodide ions were derived from mobile ions in the MAPbI$_3$ films.

For more detailed analyses, the thermally degraded PSCs were characterized by high-resolution TEM (HRTEM) and fast Fourier-transform (FFT) analysis (Fig. 5). Figure 5b–d show TEM images of the MAPbI$_3$/spiro-OMeTAD interface, MAPbI$_3$ proximal to spiro-OMeTAD, and spiro-OMeTAD proximal to MAPbI$_3$, respectively. The lattice parameter of MAPbI$_3$ was determined to be about 0.31 nm, which is similar to the (004) or (220) tetragonal phase of MAPbI$_3$[42]. Although iodine partially diffused into spiro-OMeTAD, the crystal lattice of MAPbI$_3$ did not change with thermal treatment at 85 °C for 2 h. There were no observations of changes to the crystal lattice and diffraction pattern due to iodine diffusion in spiro-OMeTAD (Fig. 5d). Spiro-OMeTAD crystallizes at 100 °C, resulting reduced conductivity[43]. However, no spiro-OMeTAD crystallization was observed by FFT and XRD in this study (Figure S6). Since the diffraction pattern of spiro-OMeTAD was not observed, it is evident that the iodine was present in spiro-OMeTAD as ions rather than precipitates. Thus, iodine as an ion reacts easily with spiro-OMeTAD, resulting in reduction of spiro-OMeTAD$^+$. Since ion migration is fast in organic materials, such as small molecules, this migration may be the origin of the efficiency drop of PSCs at high temperatures within a short time period rather than decomposition of the perovskite. As supporting evidence, it was reported that thermally stable PSCs with HTM-free structures (i.e., without an organic HTM) experienced a <10% efficiency drop[30]. These researchers developed PSCs with an m-TiO$_2$/ZrO$_2$/MAPbI$_3$ structure without an organic HTM, thereby achieving greatly enhanced thermal stability. Furthermore, several structures with a barrier film between MAPbI$_3$ and spiro-OMeTAD have been reported[12, 44]. Although the role of the barrier film was to protect the layers from moisture, it was proposed that the film could also block the diffusion of iodide ions.

To verify the changes in the chemical bonding of spiro-OMeTAD, the binding energies were assessed by X-ray photoelectron spectroscopy (XPS) at varying temperatures (Fig. 6). The results for spiro-OMeTAD and MAPbI$_3$/spiro-OMeTAD samples were compared after treatment at 25 and 85 °C. A N 1s species with an energy of 399.8 eV was observed and corresponds to C–N in spiro-OMeTAD and the imide group in Li-TFSI[32, 45].

After treatment at 85 °C, N 1s of spiro-OMeTAD remained and a peak at 401.2 eV appeared in the MAPbI$_3$/spiro-OMeTAD structure. This binding energy corresponds to amine groups such as CH$_3$NH$_2$[46]. It is thought that the diffused MAI separated into CH$_3$NH$_2$ and HI at 85 °C[10, 47]. Thus, not only I$^-$ but also MA$^+$ from MAPbI$_3$ diffused under thermal conditions. In contrast with the N 1s peaks, the other C, Pb, and I bonds changed only marginally (Figure S7).

From the TEM, EDX, and XPS data, MAI-poor region may form at the MAPbI$_3$/spiro-OMeTAD interface. Since the MAI-poor film in MAPbI$_3$ acts as an n-type film because of an increase in the Fermi level[48], energy barrier bands formed at the MAPbI$_3$/spiro-OMeTAD interface because of energy band bending. When a hole is collected during operation, the energy barriers block and rectify the motion of the hole. Thus, these energy barriers can also hinder the collection of charge carriers, thereby decreasing the solar cell performance.

In order to confirm the effect of spiro-OMeTAD degradation, the PSC performances were compared depending on the spiro-OMeTAD conditions (Fig. 7). The following procedure was used for re-deposition of spiro-OMeTAD: (1) I–V measurements of the pristine condition; (2) I–V measurements after thermal treatment
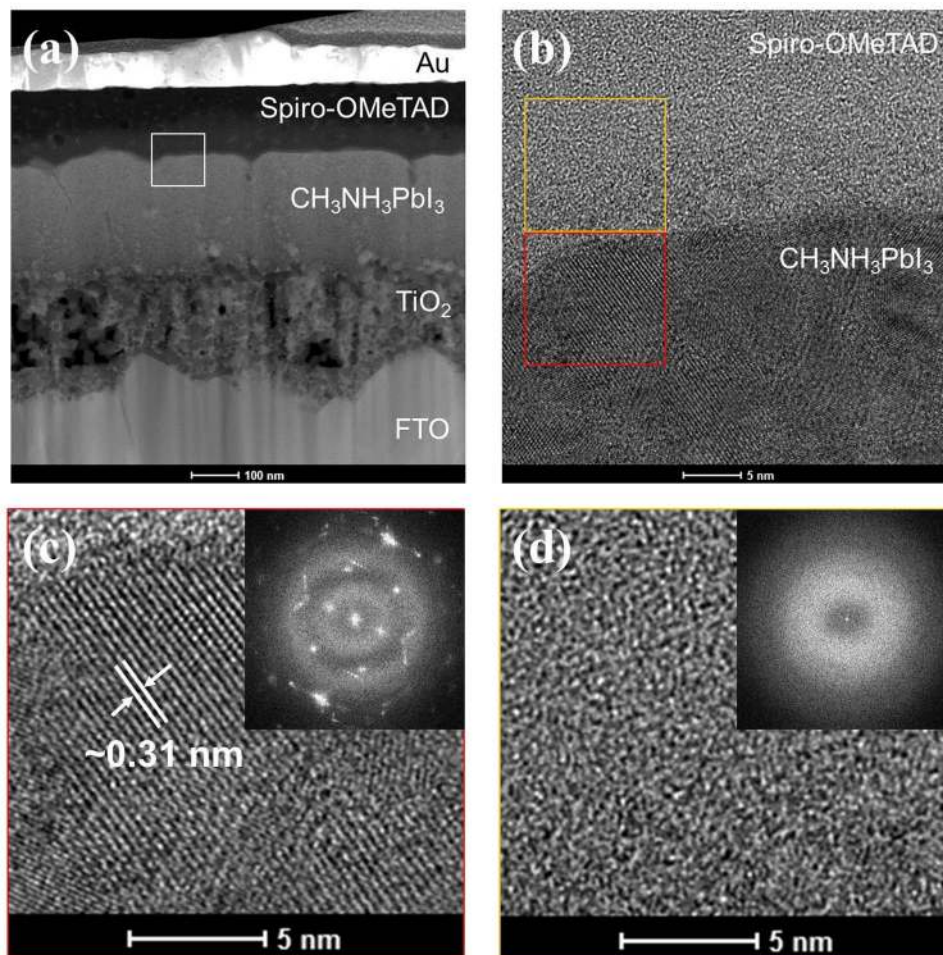
Figure 5. (**a**) TEM micrograph of FTO/TiO$_2$/MAPbI$_3$/spiro-OMeTAD/Au sample. (**b**) High resolution TEM image of MAPbI$_3$/spiro-OMeTAD interface shown in (**a**): white square; (**c,d**) highly magnified TEM image of MAPbI$_3$ and spiro-OMeTAD shown in (**b**): red square and yellow square, respectively. Inset images show the fast Fourier transform pattern.

at 85 °C for 50 h under inert Ar; (3) I–V measurements after recovery at 25 °C for 500 h under inert Ar; and (4) I–V measurements after removal of Au and spiro-OMeTAD and after re-deposition of spiro-OMeTAD and Au. Initially, the average efficiency of the PSCs was 15%, and, despite a 500 h recovery time, the PSC efficiency remained around 7% after thermal treatment. However, after re-deposition of spiro-OMeTAD and Au, the PSC performance almost completely recovered to the initial values. These results indicate that spiro-OMeTAD was degraded at 85 °C rather than MAPbI$_3$. In other words, the main reason for the degradation of the PSC performance at 85 °C was the degradation of spiro-OMeTAD. This degradation and recovery behavior was observed regardless of the atmosphere, i.e., ambient air or inert Ar (Figure S8). Because thermal diffusion of ions is not dependent on the atmosphere, the rapid efficiency drop at 85 °C was attributed to spiro-OMeTAD degradation caused by ion diffusion rather than decomposition of MAPbI$_3$.

To prevent ion diffusion, the stability of m-TiO$_2$/MAPbI$_3$/MoO$_x$/spiro-OMeTAD with a <10 nm MoO$_x$ interface layer was evaluated at 85 °C (Figure S9). The results showed slight moderation of the thermal degradation. The MoO$_x$-inserted cell showed a lower initial efficiency because MoOx is not suitable as an interface layer between MAPbI$_3$ and spiro-OMeTAD with respect to electrical properties (Table S1). Although MoO$_x$ is not an ideal diffusion barrier, the reduction in degradation was attributed to hindered ion migration. A reduction in iodine diffusion was confirmed by TOF-SIMS (Figure S10).

Ion migration into spiro-OMeTAD degrades the electrical properties of spiro-OMeTAD through reduction and decreases charge-carrier collection through the formation of energy barriers. Because this kind of ion migration can occur during operation outdoor or in other external environments, the compositional and structural design of PSCs must be optimized to achieve long-term stability.

In this study, to determine the cause of the reduction in efficiency of spiro-OMeTAD–based PSCs upon thermal exposure at 85 °C for a short time period, we investigated the thermal behavior of spiro-OMeTAD and MAPbI$_3$/spiro-OMeTAD films. The results showed that spiro-OMeTAD was highly oxidized at 85 °C; in contrast, the oxidation of spiro-OMeTAD in MAPbI$_3$/spiro-OMeTAD was hindered by diffusion of iodide ions from
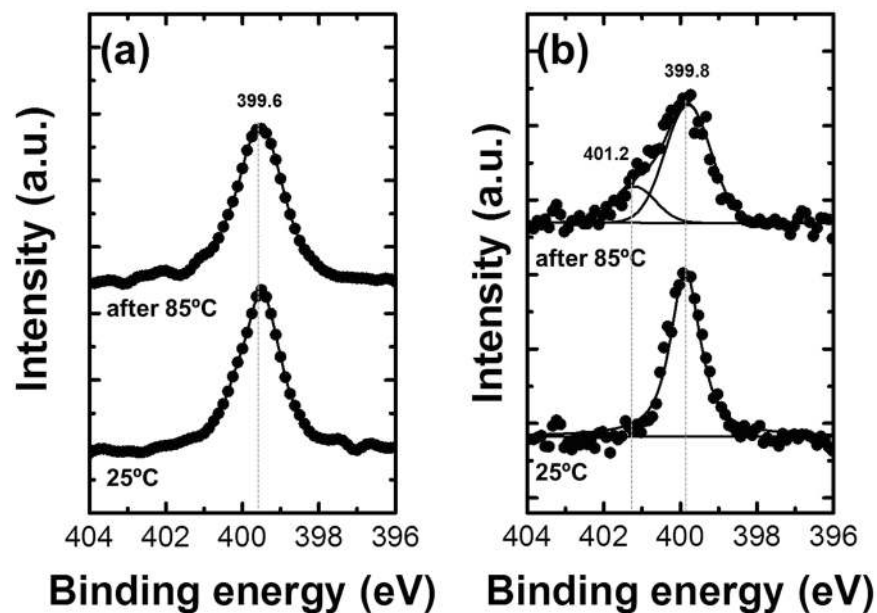
Figure 6. N 1s XPS narrow scan spectra of (**a**) spiro-OMeTAD only and (**b**) MAPbI$_3$/spiro-OMeTAD as-prepared (25 °C) and after thermal treatment (85 °C). XPS data were acquired from the spiro-OMeTAD side.
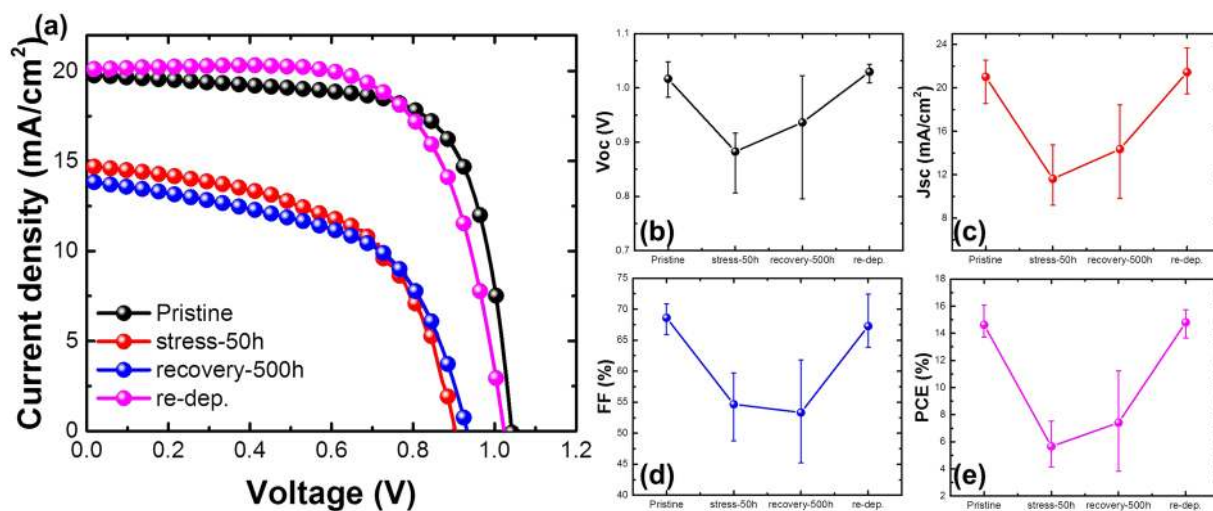

Figure 7. Step-by-step procedures for the re-deposition of spiro-OMeTAD: 1) pristine, 2) after thermal treatment at 85 °C for 50 h, 3) after recovery at 25 °C for 500 h, and 4) after removal of Au and spiro-OMeTAD followed by re-deposition of spiro-OMeTAD. (**a**) Representative I–V curves according to the spiro-OMeTAD conditions. Average values of seven cells with procedures plotted to (**b**) V_{oc}, (**c**) J_{sc}, (**d**) FF, and (**e**) PCE.

MAPbI$_3$ at temperatures above room temperature, resulting in decreased conductivity of spiro-OMeTAD. Iodide ions diffuse easily into spiro-OMeTAD and act as reducing agents for spiro-OMeTAD at elevated temperatures. Since CH$_3$NH$_2$ was detected on the surface of spiro-OMeTAD, it was concluded that iodide ions migrated in the form of MAI. The observed re-deposition of spiro-OMeTAD rather than degraded spiro-OMeTAD suggests that the main reason for the degradation of PSCs at 85 °C was degradation of spiro-OMeTAD rather than decomposition of MAPbI$_3$. This thermally activated ion diffusion may occur during outdoor operation of PSCs and can decrease the conversion efficiency. Therefore, the compositional and constructional design of perovskites or PSCs must be considered to enhance the thermal and overall stability of PSCs.

References
1. Kojima, A., Techima, K., Shirai, Y. & Miyasaka, T. Organometal Halide Perovskites as Visible-Light Sensitizers for Photovoltaic Cells. *J. Am. Chem. Soc.* **131**, 6050–6051 (2009).
2. Kim, H.-S. *et al.* Lead Iodide Perovskite Sensitized All-Solid-State Submicron Thin Film Mesoscopic Solar Cell with Efficiency Exceeding 9%. *Sci. Rep.* **2**, 591 (2012).

3. Burschka, J. *et al*. Sequential deposition as a route to high-performance perovskite-sensitized solar cells. *Nature* **499**, 316–319 (2013).
4. Jeon, N. J. *et al*. I. Compositional engineering of perovskite materials for high-performance solar cells. *Nature* **517**, 476–480 (2015).
5. Saliba, M. *et al*. Cesium-containing triple cation perovskite solar cells: improved stability, reproducibility and high efficiency. *Energy Environ.* **9**, 1989–1997 (2016).
6. NREL. Best Research-Cell Efficiencies, http://www.nrel.gov/pv/assets/images/efficiency_chart.jpg (Date of access: 12/08/2016).
7. Ahn, N. *et al*. Highly Reproducible Perovskite Solar Cells with Average Efficiency of 18.3% and Best Efficiency of 19.7% Fabricated via Lewis Base Adduct of Lead(II) Iodide. *J. Am. Chem. Soc.* **137**, 8696–8699 (2015).
8. Chen, Q. *et al*. Under the spotlight: The organic-inorganic hybrid halide perovskite for optoelectronic application. *Nano Today* **10**, 355–396 (2015).
9. Hwang, I., Jeong, I., Lee, J., Ko, M. J. & Yong, K. Enhancing Stability of Perovskite Solar Cells to Moisture by the Facile Hydrophobic Passivation. *ACS Appl. Mater. Interfaces* **7**, 17330–17336 (2015).
10. Conings, B. *et al*. Intrinsic Thermal Instability of Methylammonium Lead Trihalide Perovskite. *Adv. Energy Mater.* **5**, 1500477 (2015).
11. Habisreutinger, S. N. *et al*. Carbon Nanotube/Polymer Composites as a Highly Stable Hole Collection Layer in Perovskite Solar Cells. *Nano Lett.* **14**, 5561–5568 (2014).
12. Niu, G. *et al*. Study on the stability of $CH_3NH_3PbI_3$ films and the effect of post-modification by aluminum oxide in all-solid-state hybrid solar cells. *J. Mater. Chem. A* **2**, 705–710 (2014).
13. Leijtens, T. *et al*. Overcoming ultraviolet light instability of sensitized TiO_2 with meso-superstructured organometal tri-halide perovskite solar cells. *Nat. Commun.* **4**, 2885 (2013).
14. Bae, S. *et al*. Electric-Field-Induced Degradation of Methylammonium Lead Iodide Perovskite Solar Cells. *J. Phys. Chem. Lett.* **7**, 3091–3096 (2016).
15. Azpiroz, J. M., Mosconi, E., Bisquert, J. & Angelis, F. D. Defect migration in methylammonium lead iodide and its role in perovskite solar cell operation. *Energy Environ. Sci.* **8**, 2118–2127 (2015).
16. Yang, J., Siempelkamp, B. D., Mosconi, E., Angelis, F. D. & Kelly, T. L. Origin of the Thermal Instability in $CH_3NH_3PbI_3$ Thin Films Deposited on ZnO. *Chem. Mater.* **27**, 4229–4236 (2015).
17. Nguyen, W. H., Bailie, C. D., Unger, E. L. & McGehee, M. D. Enhancing the Hole-Conductivity of Spiro-OMeTAD without Oxygen or Lithium Salts by Using Spiro$(TFSI)_2$ in Perovskite and Dye-Sensitized Solar Cells. *J. Am. Chem. Soc.* **136**, 10996–11001 (2014).
18. Li, M.-H. *et al*. Novel spiro-based hole transporting materials for efficient perovskite solar cells. *Chem. Commun.* **51**, 15518–15521 (2015).
19. Kwon, Y. S., Lim, J., Yun, H.-J., Kim, Y.-H. & Park, T. A diketopyrrolopyrrole-containing hole transporting conjugated polymer for use in efficient stable organic–inorganic hybrid solar cells based on a perovskite. *Energy Environ. Sci.* **7**, 1454–1460 (2014).
20. Gatti, T. *et al*. Boosting Perovskite Solar Cells Performance and Stability through Doping a Poly-3(hexylthiophene) Hole Transporting Material with Organic Functionalized Carbon Nanostructures. *Adv. Funct. Mater.* **26**, 7443–7453 (2016).
21. Bai, Y. *et al*. Enhancing Stability and Efficiency of Perovskite Solar Cells with Crosslinkable Silane-Functionalized and Doped Fullerene. *Nature Comm* **7**, 12806 (2016).
22. Burschka, J. *et al*. Tris(2-(1H-pyrazol-1-yl)pyridine)cobalt(III) as p-Type Dopant for Organic Semiconductors and Its Application in Highly Efficient Solid-State Dye-Sensitized Solar Cells. *J. Am. Chem. Soc.* **133**, 18042–18045 (2011).
23. Leijtens, T., Lim, J., Teuscher, J., Park, T. & Snaith, H. J. Charge Density Dependent Mobility of Organic Hole-Transporters and Mesoporous TiO_2 Determined by Transient Mobility Spectroscopy: Implications to Dye-Sensitized and Organic Solar Cells. *Adv. Mater.* **25**, 3227 (2013).
24. Abate, A. *et al*. Lithium salts as "redox active" p-type dopants for organic semiconductors and their impact in solid-state dye-sensitized solar cells. *Phys. Chem. Chem. Phys.* **15**, 2572–2579 (2013).
25. Li, W. *et al*. Montmorillonite as bifunctional buffer layer material for hybrid perovskite solar cells with protection from corrosion and retarding recombination. *J. Mater. Chem. A* **2**, 13587–13592 (2014).
26. Niu, G., Guo, X. & Wang, L. Review of recent progress in chemical stability of perovskite solar cells. *J. Mater. Chem. A* **3**, 8970–8980 (2015).
27. Etgar, L. *et al*. Mesoscopic $CH_3NH_3PbI_3/TiO_2$ Heterojunction Solar Cells. *J. Am. Chem. Soc.* **134**, 17396–17399 (2012).
28. Wang, S., Yuan, W. & Meng, Y. S. Spectrum-Dependent Spiro-OMeTAD Oxidization Mechanism in Perovskite Solar Cells. *ACS Appl. Mater. Interfaces* **7**, 24791–24798 (2015).
29. Carrillo, J. *et al*. Ionic reactivity at Contacts and Aging of Methylammonium Lead Triiodide Perovskite Solar Cell. *Adv. Energy Mater.* **6**, 1502246 (2016).
30. Li, X. *et al*. Outdoor Performance and Stability under Elevated Temperatures and Long-Term Light Soaking of Triple-Layer Mesoporous Perovskite Photovoltaics. *Energy Technol* **3**, 551–555 (2015).
31. Li, X. *et al*. Improved performance and stability of perovskite solar cells by crystal crosslinking with alkylphosphonic acid ω-ammonium chlorides. *Nature Chem* **7**, 703–711 (2015).
32. Hawash, Z., Ono, L. K., Raga, S. R., Lee, M. V. & Qi, Y. Air-Exposure Induced Dopant Redistribution and Energy Level Shifts in Spin-Coated Spiro-MeOTAD Films. *Chem. Mater.* **27**, 562–569 (2015).
33. Liu, F. *et al*. Perovskite Solar Cells: Is Excess PbI_2 Beneficial for Perovskite Solar Cell Performance? *Adv. Energy Mater.* **6**, 1502206 (2016).
34. Cao, D. H. *et al*. Remnant PbI_2, an unforeseen necessity in high-efficiency hybrid perovskite-based solar cells?[a]. *Appl. Mater.* **2**, 091101 (2014).
35. Fantacci, S., Angelis, F. D., Nazeeruddin, M. K. & Gratzel, M. Electronic and Optical Properties of the Spiro-MeOTAD Hole Conductor in Its Neutral and Oxidized Forms: A DFT/TDDFT Investigation. *J. Phys. Chem. C* **115**, 23126–23133 (2011).
36. Polander, L. E. *et al*. Hole-Transport Material Variation in Fully Vaccum Deposited Perovskite Solar Cells. *APL. Materials* **2**, 081503 (2014).
37. Haruyama, J., Sodeyama, K., Han, L. & Tateyama, Y. First-Principles Study of Ion Diffusion in Perovskite Solar Cell Sensitizers. *J. Am. Chem. Soc.* **137**, 10048–10051 (2015).
38. Yang, T.-Y., Gregori, G., Pellet, N., Grätzel, M. & Maier, J. The Significance of Ion Conduction in a Hybrid Organic–Inorganic Lead-Iodide-Based Perovskite Photosensitizer. *J. Angew. Chem.* **127**, 8016–8021 (2015).
39. Liu, Y. *et al*. A dopant-free organic hole transport material for efficient planar heterojunction perovskite solar cells. *J. Mater. Chem. A* **3**, 11940–11947 (2015).
40. Divitini, G. *et al*. *In situ* observation of heat-induced degradation of perovskite solar cells. *Nature Energy* **1**, 15012 (2016).
41. Shao, Y. *et al*. Grain Boundary Dominated Ion Migration in Polycrystalline Organic-Inorganic Halide Perovskite Films. *Energy Environ. Sci.* **9**, 1752–1759 (2016).
42. Son, D.-Y. *et al*. Self-formed grain boundary healing layer for highly efficient $CH_3NH_3PbI_3$ perovskite solar cells. Nature. *Energy* **1**, 16081 (2016).
43. Malinauskas, T. *et al*. Enhancing Thermal Stability and Lifetime of Solid-State Dye-Sensitized Solar Cells via Molecular Engineering of the Hole-Transporting Material spiro-OMeTAD. *ACS Appl. Mater. Interfaces* **7**, 11107–11116 (2015).
44. Yun, J. H. *et al*. Synergistic enhancement and mechanism study of mechanical and moisture stability of perovskite solar cells introducing polyethylene-imine into the $CH_3NH_3PbI_3$/HTM interface. *J. Mater. Chem. A* **3**, 22176 (2015).

45. Dedryvère, R. *et al*. XPS Valence Characterization of Lithium Salts as a Tool to Study Electrode/Electrolyte Interfaces of Li-Ion Batteries. *J. Phys. Chem. B* **110**, 12986–12992 (2006).
46. Calloni, A. *et al*. Stability of Organic Cations in Solution-Processed CH$_3$NH$_3$PbI$_3$ Perovskites: Formation of Modified Surface Layers. *J. Phys. Chem. C* **119**, 21329–21335 (2015).
47. Slavney, A. H. *et al*. Chemical Approaches to Addressing the Instability and Toxicity of Lead-Halide Perovskite Absorbers. *Inorg. Chem* **56**, 46–55 (2016).
48. Wang, Q. *et al*. Qualifying composition dependent p and n self-doping in CH$_3$NH$_3$PbI$_3$. *J. Appl. Phys. Lett.* **105**, 163508 (2014).

Acknowledgements

Author Contributions

Seongtak Kim contributed to the overall project and wrote an entire manuscript. Soohyun Bae, Kyung Dong Lee and Hyunho Kim performed the data analysis. Sang-Won Lee and Kyungjin Cho fabricated the perovskite solar cell and characterized the J-V performances. Sungeun Park, Guhan Kwon, Seh-Won Ahn and Heon-Min Lee discussed the results and commented on the manuscript, Yoonmook Kang, Hae-Seok Lee, and Donghwan Kim designed and supervised this project. All authors reviewed the manuscript.

Additional Information

Supplementary information accompanies this paper at doi:10.1038/s41598-017-00866-6

Competing Interests: The authors declare that they have no competing interests.

Publisher's note: Springer Nature remains neutral with regard to jurisdictional claims in published maps and institutional affiliations.